metals

MDPI

Article

Surface Modification of the EBM Ti-6Al-4V Alloy by Pulsed Ion Beam

Natalia Pushilina [1], Ekaterina Stepanova [1,*], Andrey Stepanov [2] and Maxim Syrtanov [1]

[1] School of Nuclear Science & Engineering, National Research Tomsk Polytechnic University, 30 Lenin Avenue, 634050 Tomsk, Russia; pushilina@tpu.ru (N.P.); maxim-syrtanov@mail.ru (M.S.)
[2] Research School of High-Energy Physics, National Research Tomsk Polytechnic University, 30 Lenin Avenue, 634050 Tomsk, Russia; stepanovav@mail.ru
* Correspondence: enstepanova@tpu.ru

Abstract: The effect of surface modification of Ti-6Al-4V samples manufactured by electron beam melting (EBM) using a pulsed carbon ion beam is studied in the present work. Based on the results of XRD, SEM, and TEM analysis, patterns of changes in the microstructure and phase composition of the EBM Ti-6Al-4V alloy, depending on the number of pulses of pulsed ion beam exposure, are revealed. It was found that gradient microstructure is formed as a result of pulsed ion beam irradiation of the EBM Ti-6Al-4V samples. The microstructure of the surface layer up to 300 nm thick is represented by the ($\alpha + \alpha''$) phase. At depths of 0.3 μm, the microstructure is mixed and contains alpha-phase plates and needle-shaped martensite. The mechanical properties were investigated using methods of uniaxial tensile tests, micro- and nanohardness measurements, and tribological tests. It was shown that surface modification by a pulsed ion beam at an energy density of 1.92 J/cm^2 and five pulses leads to an increase in the micro- and nanohardness of the surface layers, a decrease in the wear rate, and a slight rise in the plasticity of EBM Ti-6Al-4V alloy.

Keywords: additive manufacturing; electron beam melting; titanium alloy; pulsed ion beam; phase transformation; mechanical properties

Citation: Pushilina, N.; Stepanova, E.; Stepanov, A.; Syrtanov, M. Surface Modification of the EBM Ti-6Al-4V Alloy by Pulsed Ion Beam. *Metals* **2021**, *11*, 512. https://doi.org/10.3390/met11030512

Academic Editor: Mohammad J. Mirzaali

Received: 27 February 2021
Accepted: 17 March 2021
Published: 19 March 2021

1. Introduction

Titanium alloys, due to their high strength, corrosion resistance, and low density, are widely used in medicine, aerospace, chemical and biomedical industries [1–3]. Recently, additive technologies (AT) have been actively introduced into the production of products from titanium and its alloys [4–10]. The advantages of AT over traditional methods for the production of metallic products are undeniable; high speed of production and the ability to obtain products of a unique geometric shape should be noted as the most significant [4]. Therefore, the use of AT makes it possible to create materials of a new generation with a unique set of properties [4–11]. However, for the widespread introduction of AT, it is necessary to solve the problems of porosity [7,8], residual stresses, and anisotropy of the properties of materials [9–13] produced using AT. Optimization of the properties of additively manufactured materials can be achieved by several methods. On the one hand, one such method may be the selection of the optimal mode of sample production. This is caused by the fact that there are a large number of parameters and scanning strategies that can be changed and optimized to control the microstructure and properties of metallic materials during electron beam melting (EBM) [14]. The most commonly varied parameters are voltage, beam current, focus, frequency, and scan strategy. On the other hand, one of the effective ways to improve the mechanical properties of additively manufactured metallic materials, including titanium alloys, is to carry out additional post-processing. These types of processing include hot isostatic pressing [15,16] and heat treatment [17–19]. It is also proposed to carry out additional treatment using pulsed

electron beam processing [20], continuous electron beam scanning treatment [21], and laser polishing [22].

Surface treatment of parts from titanium alloys with charged particle beams (ion implantation, processing with powerful ion beams, processing with high-current pulsed electron beams) occupies a special place. This is due to its ability to modify surface layers without changing the physicochemical state of the materials in the bulk of the parts. The effectiveness of the application of powerful pulsed ion beams and ion implantation for processing products from titanium and its alloys has already been proven in many works [23–36]. It was shown that, as a result of pulsed ion beam exposure, it is possible to reduce surface roughness [23], form a gradient microstructure [26,27], increase mechanical properties [28–33], and improve corrosion resistance [34,35]. At the same time, the process of material surface treatment by pulsed ion beam is also characterized by a number of limitations. For example, it is quite difficult to apply this type of processing to samples with complex geometry; in addition, during pulsed charged particle beam treatment of internal surfaces, serious technological problems often arise [36].

At the same time, studies on the modification of titanium parts manufactured by electron beam melting using pulsed ion beams, in order to improve their properties, have not been carried out practically. The purpose of the present work is to establish patterns of the effect of ion modification modes on the structure, phase composition, and mechanical properties of the EBM Ti-6Al-4V alloy.

2. Materials and Methods

2.1. Sample Preparation

In this work, samples were obtained using the EBM method from a powder of the Ti-6Al-4V composition manufactured by NORMIN Company (Normin, Borovichi, Russia) [37]. The average powder size ranged from 50 to 90 μm. Samples were produced using an electron beam melting 3D printer designed at the National Research Tomsk Polytechnic University (Tomsk, Russia) [37]. The experimental parameters were as follows: an accelerating voltage of 40 kV, and a melting current of 15 mA. Sample billets were obtained in the form of plates with dimensions of 50 × 20 × 3 mm^3.

The surface of the samples was modified by a pulsed beam of carbon ions (pulse duration of 80 ns, energy of 200 keV, current density of 120 A/cm^2, and energy density of 1.92 J/cm^2) using a TEMP high-current pulse accelerator (TPU, Tomsk, Russia) [38]. Two modification modes with a different number of carbon ion beam pulses (N) were used: mode 1 (N = 5) and mode 2 (N = 10).

2.2. Experimental Methods

The as-built samples were ground using 2000 grid SiC paper, polished using 1 mm diamond paste to completely remove surface defects, and etched by an etchant composed of 1 mL HF, 5 mL HNO_3, and 10 mL H_2O. The study of the microstructure of the sample surface and fractographic analysis were carried out using a system with focused electronic and ion beams—Quanta 200 3D (FEI Company, Hillsboro, OR, USA). A JEM-2100F (JEOL, Akishima, Tokyo, Japan) transmission electron microscope was employed for the microstructural characterization of the samples. The study was conducted at an accelerating voltage of 200 kV. The samples were prepared by ion milling using an EM-09100IS Ion Slicer (JEOL, Akishima, Tokyo, Japan). During preparation, argon was used as the working gas, the accelerating voltage was 8 kV, and the etching angle was 1.5–4°. The ion milling process was controlled by a charged coupled device (CCD) camera (JEOL, Akishima, Tokyo, Japan).

The study of the structural and phase state and the determination of crystal lattice parameters and internal stresses were carried out using an XRD-7000S diffractometer (Shimadzu, Kyoto, Japan), using Bragg–Brentano geometry; the angles under study were 30–80°, and the scanning speed was 10.0 deg/min. A PowderCell 2.4 software package (Federal Institute for Materials Research and Testing, Berlin, Germany) was used to identify

the diffraction pattern. The volume fraction of the β phase was calculated using a Reference Intensity Ratio (RIR). According to this method, the content of the β phase could be evaluated by the following equation:

$$w_k = \frac{I_k^{max}/RIR_k}{\sum_i I_i^{max}/RIR_i} \quad (1)$$

where w_k—volume fraction of the required phase; I^{max}—the most intense peak of the phase; *RIR*—reference intensity ratio of the phase.

Measurement of wear resistance and friction coefficient was carried out with a "High-Temperature Tribometer" installation (CSEM, Neuchâtel, Switzerland). The following parameters for determination of wear resistance were used: number of revolutions—2000; indenter—tungsten carbide; applied force—2 N. The wear track area was measured with a STIL Micromeasure 3D non-contact optical profilometer. Uniaxial tensile tests were carried out at room temperature using an INSTRON 3369 electromechanical testing machine (Instron, Wycombe, UK) with an initial strain rate of 6.9×10^{-3} s^{-1}. Test specimens shaped as double blades with dimensions of the working part of $5 \times 5 \times 1$ mm^3 [39] were cut from billets by the electrospark method. For each series of samples prepared using different processing modes, at least 5 samples were tested. Vickers microhardness was measured on the polished surface of samples with a load of 0.5 *N* using a KB 30S (Pruftechnik, Ismaning, Germany) microhardness tester. Nanohardness and Young's modulus were determined using a tabletop nanoindentation system (CSM Instruments, Peseux, Switzerland). The load on the indenter was 400 mN and the maximum analysis depth was about 2 μm. At least 20 measurements were taken for each sample.

3. Results

3.1. Microstructure and Phase Composition

According to the results of the scanning electron microscopy, the structure of the manufactured samples is characterized by the presence of relatively large initial β-grains, the internal volume of which is represented by α-plates combined in colonies (Figure 1a). A study of the pattern of the sample surface relief after pulsed ion beam (PIB) exposure has shown that, in the zone of the ion beam action, the material is heated and melted, and partially evaporates.

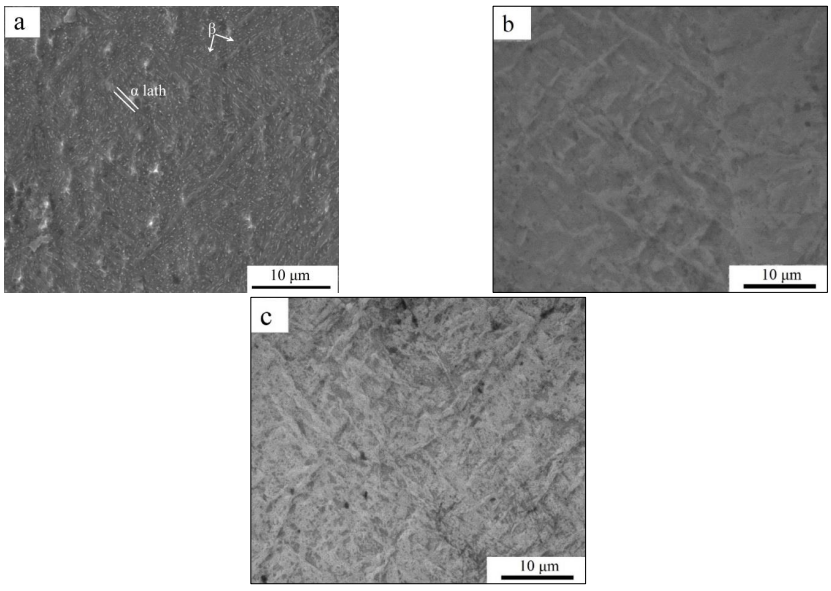

Figure 1. SEM images of electron beam melting (EBM) Ti-6Al-4V alloys: as-built samples (**a**), after pulsed ion beam (PIB) exposure (mode 1) (**b**), after PIB exposure (mode 2) (**c**).

After PIB exposure, a lamellar relief is observed on the modified sample surface. The formation of such a relief may be connected with the martensitic transformation that occurs in (α + β) titanium alloys quenched from the region of the β phase. Plastic deformation during sliding under compressive (parallel to the surface) quasistatic stresses during recrystallization, after the end of the pulsed beam exposure, can be another possible reason for the formation of the surface relief after PIB [40]. Single microcraters are present on the surface of specimens modified with PIB, and their fractions increase with the rise in the number of exposure pulses from 5 to 10 pulses (Figure 1b,c).

A more detailed study of the transverse sections of the samples was carried out using transmission electron microscopy (Figures 2–5). The structure of the as-built EBM Ti-6Al-4V samples is represented by a lamellar α phase with a transverse plate size of 120–500 nm (Figure 2), and a β-phase in the form of plates and globular grains 0.1–0.2 μm in size embedded in the grain boundaries of the α-phase. TEM studies have shown that structural changes after PIB exposure extend to a depth of more than 5 μm. It is clearly seen that the structure formed as a result of PIB modification has several distinct zones (Figure 3). In the first zone (Layer 1 in Figure 3a), with a thickness of ~300 nm, the formation of a lamellar (α + α″) phase with a transverse plate size of 30–10 nm was observed.

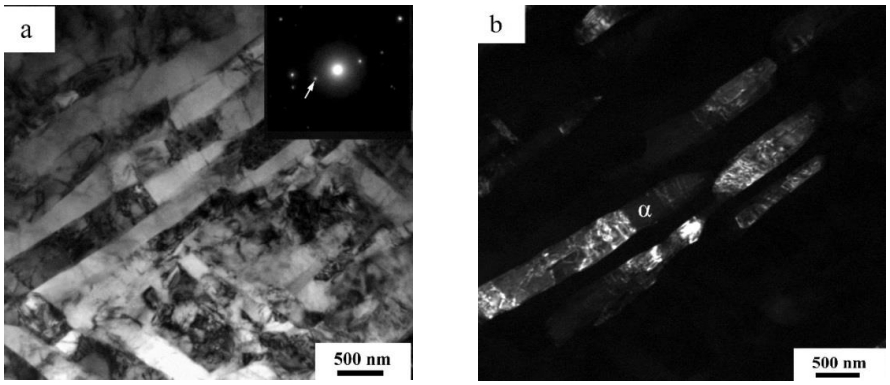

Figure 2. Transmission electron microscopy (TEM) images of the as-built specimen of the EBM Ti-6Al-4V alloy: bright-field image and corresponding microdiffraction (**a**), dark-field image in the $(100)_{\alpha\text{-Ti}}$ reflection (indicated by an arrow) (**b**).

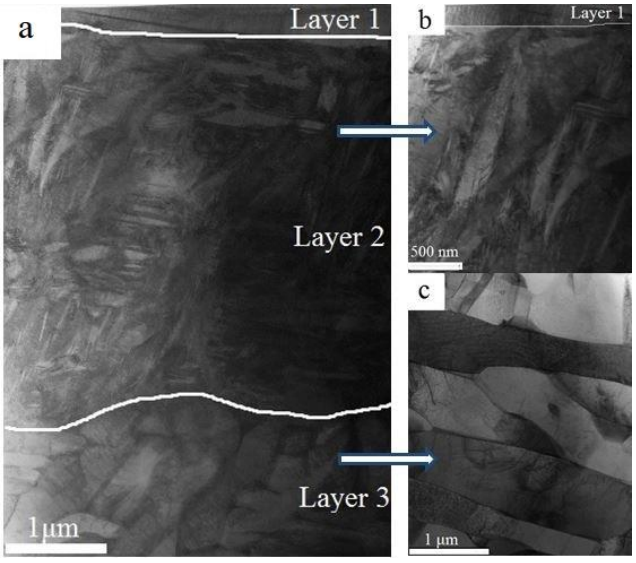

Figure 3. Microstructure of the EBM Ti-6Al-4V alloy samples after PIB exposure at various depths: characteristic zones with different microstructure designated as Layers 1, 2, 3 (**a**), scanning transmission electron microscopy (STEM) images of Layers 1 and 2 (**b**), STEM image of Layer 3 (**c**).

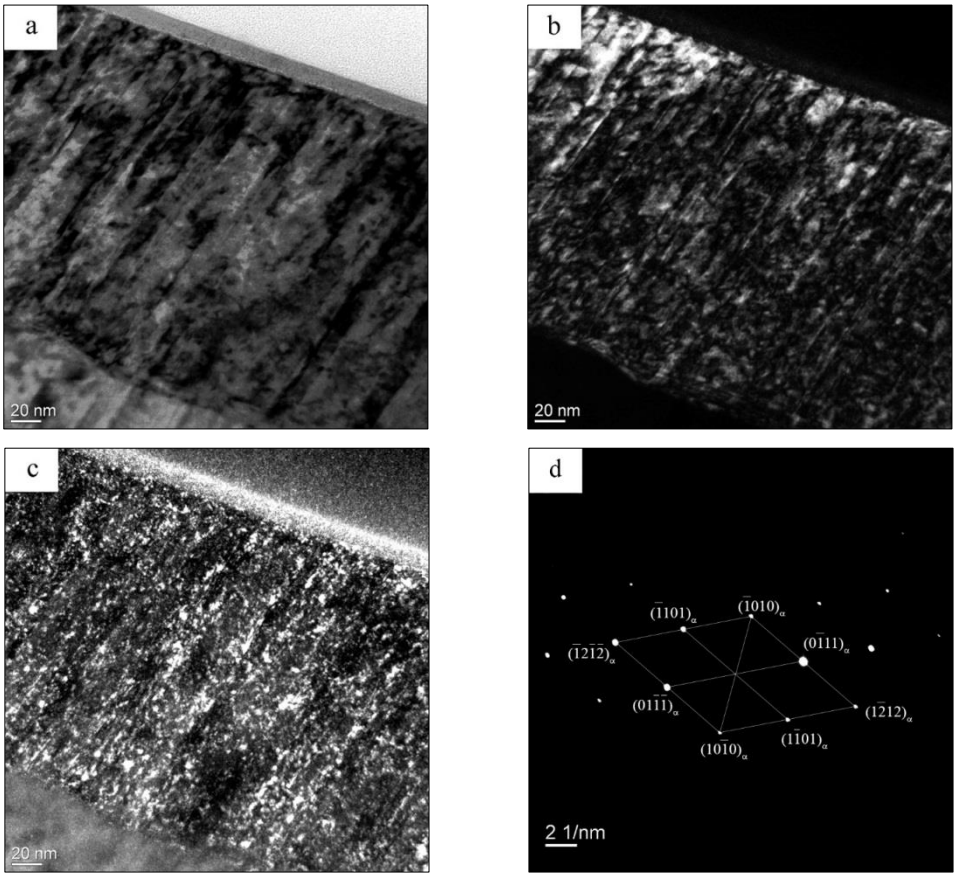

Figure 4. TEM images of the EBM Ti-6Al-4V samples after PIB irradiation: structure of the surface layer 1: bright-field image (**a**), dark-field images in the $(0\bar{1}11)$ (**b**), $(\bar{1}010)$ (**c**), reflections, corresponding microdiffraction (**d**).

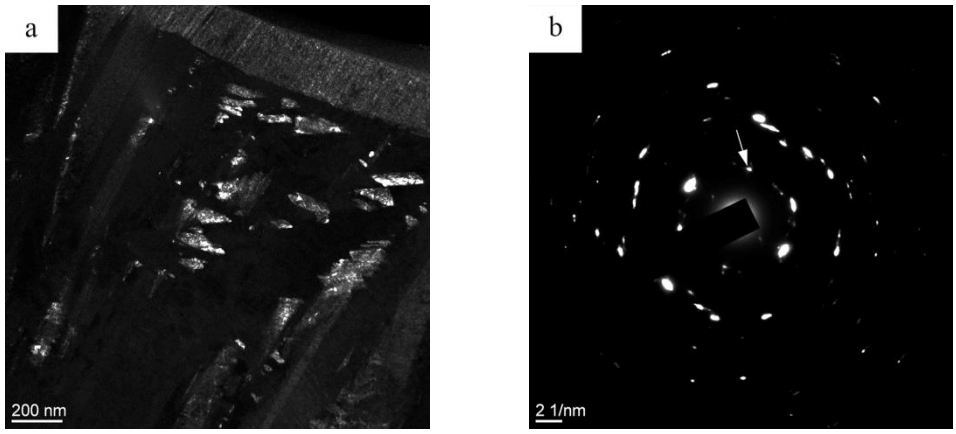

Figure 5. Microstructure of surface layer 2 of the EBM Ti-6Al-4V samples after PIB irradiation: dark-field image in the $(220)_{\alpha''\text{-Ti}}$ reflection (indicated by an arrow in Figure 2b) (**a**), and microdiffraction (**b**).

TEM images of the next layer of microstructure (Layer 2 in Figure 3a) are shown in Figure 5. It can be seen that this layer is also characterized by an acicular structure; in the layer, a (α'' + $\alpha(\alpha')$ + β) state was formed as a result of PIB exposure. The average thickness of the layer is 4 μm. At a depth of more than 4 μm (Layer 3 in Figure 3a–c), the microstructure of irradiated samples contains ($\alpha(\alpha')$ + β) phases and does not differ significantly from the microstructure of as-built specimens. In the bulk of the material, the

microstructure is represented by α phase plates, the thickness of which varies from 0.12 to 1 μm, and the beta phase in the form of interlayers.

According to X-ray diffraction analysis data (Shimadzu, Kyoto, Japan), the α-phase of titanium, with a hexagonal close-packed crystal structure, and the β-phase, with a body-centered cubic crystalline modification, are observed in the as-built sample (Figure 6). The volume fraction of the β phase in the EBM Ti-6Al-4V samples was 2.7%. After irradiation by PIB, the reflections of the α-phase become broader and shift towards larger angles. In addition, it should be noted that irradiation at N = 5 pulses leads to an insignificant increase in values of microstresses from 2×10^{-3} (for as-built specimen) to 2.4×10^{-3} (for samples after PIB irradiation); with a further increase in the number of pulses to N = 10, a decrease in the values of microstresses to 1.5×10^{-3} is observed. The observed changes are associated with the supersaturation of the solid solution with alloying elements, resulting in the formation of martensitic phases. The formation of metastable phases as a result of PIB irradiation of the EBM Ti-6Al-4V alloy is due to the high heating and cooling rates of the surface from the region of the β phase.

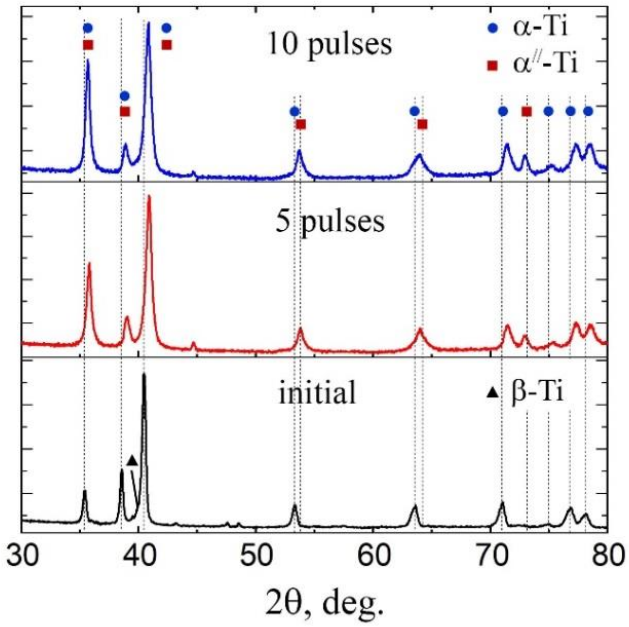

Figure 6. X-ray diffraction (XRD) patterns of the initial (as-built) sample and samples after PIB exposure.

3.2. Mechanical Properties

Tribological tests have shown that PIB modification affects the value of friction coefficient μ and character of wear scars (Figure 7).

The wear rate was calculated by equation:

$$V = 2\pi RS/Fl, \quad (2)$$

where R—track radius [mm]; S—cross-sectional area of the wear groove [mm^2]; F—value of applied load [N]; l—counterbody distance [m].

The values of the wear rate V calculated using Formula (2) are presented in Table 1. It can be seen from the data in Table 1 that irradiation of samples by PIB can lead both to a decrease in the wear rate (in the case of irradiation with N = 5) and to an increase in this value (as a result of PIB exposure with N = 10).

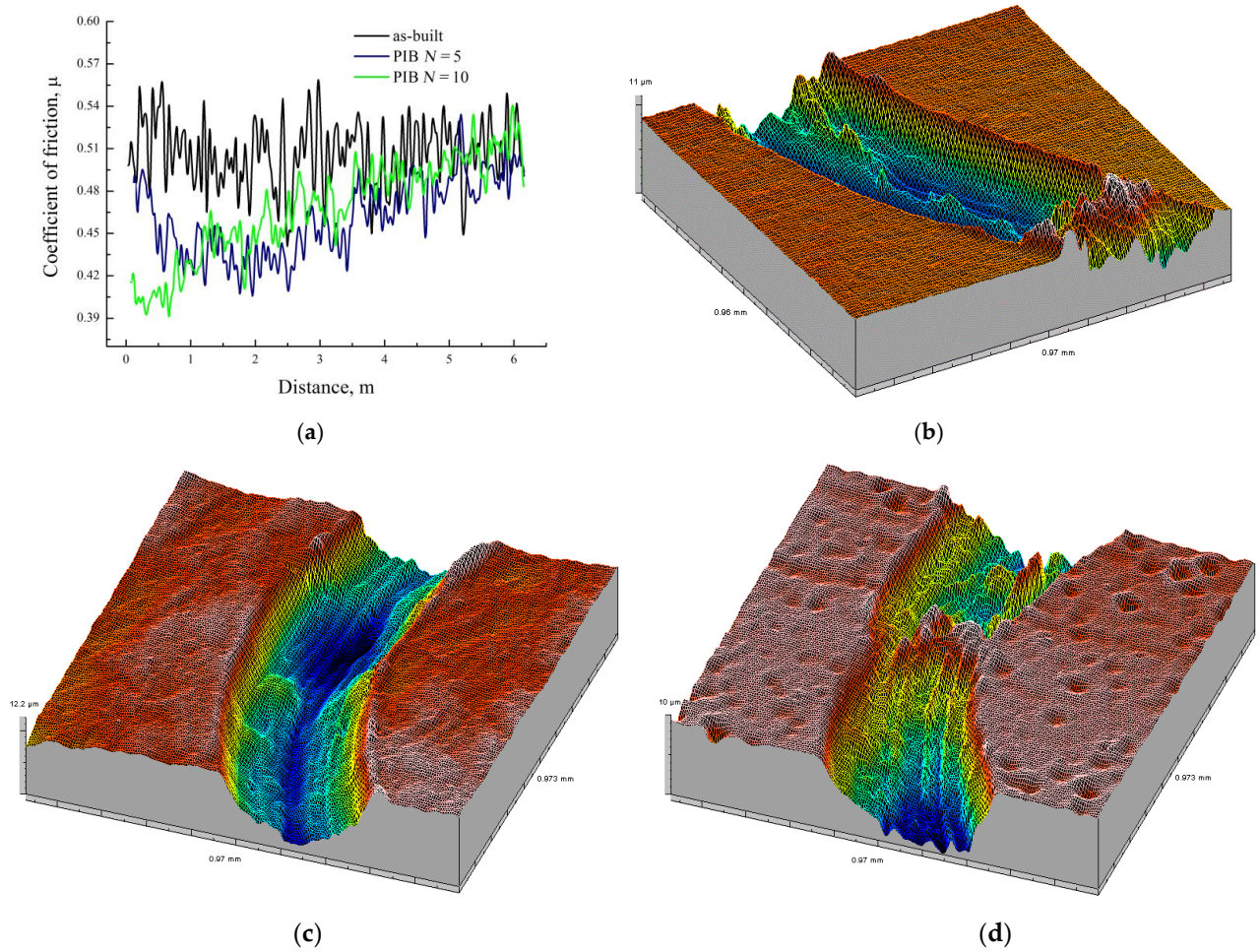

Figure 7. (**a**) Dependence of friction coefficient of the EBM Ti-6Al-4V alloy before and after PIB on distance; and wear scars for as-built sample (**b**), sample after PIB exposure (mode 1) (**c**), sample after PIB exposure (mode 2) (**d**). The average value of the friction coefficient of as-built samples of EBM Ti-6Al-4V alloy before PIB exposure was 0.49. For samples modified by PIB (N = 5 pulses), a decrease in the friction coefficient from 0.49 to 0.43 at distances of up to 2 m is observed; with further tests, the average values of the friction coefficient increase to 0.5. A feature of the samples after exposure to 10 pulses of PIB is a monotonic growth in the values of the friction coefficient with the rise in track length.

Table 1. Wear rate (V), microhardness ($H\mu$), nanohardness (H), and Young's modulus (E) of the EBM Ti-6Al-4V alloy samples before and after PIB modification.

Samples	$V \pm 0.05$, mm^3/(N·m)	$H_\mu \pm 0.2$, GPa	$H \pm 0.1$, GPa	E, GPa
as-built	0.88	3.9	4.5	108
after PIB, N = 5 pulses	0.72	6.2	5.7	134
after PIB, N = 10 pulses	0.76	6.7	4.8	103

The microhardness of the Ti-6Al-4V alloy in the initial as-built state was 3.9 GPa. Modification of the samples with a pulsed ion beam leads to an increase in the microhardness values: in the case of irradiation with five pulses, up to 6.2 GPa, and, for N = 10, up to 6.7 GPa.

Figure 8a represents load–depth nanoindentation curves for the samples of the EBM Ti-6Al-4V alloy in the initial state and after PIB irradiation. It can be seen (Figure 8a, Table 1) that the highest values of nanohardness are characteristic for samples irradiated with carbon PIB (mode 1). Such a rise in nanohardness as a result of PIB exposure is caused by the refinement of the microstructure and structural and phase changes in the surface layers of the material, as a result of high-speed heating to melting temperature and cooling during irradiation with a pulsed beam. A further rise in the number of pulses

(up to N = 10) leads to a decrease in the values of nanohardness. In addition, mechanical studies have shown that an increase in Young's modulus is observed upon irradiation with five pulses of PIB (Table 1). Thus, surface modification by PIB leads to the formation of a gradient structure, the properties of which change significantly depending on the distance to the surface.

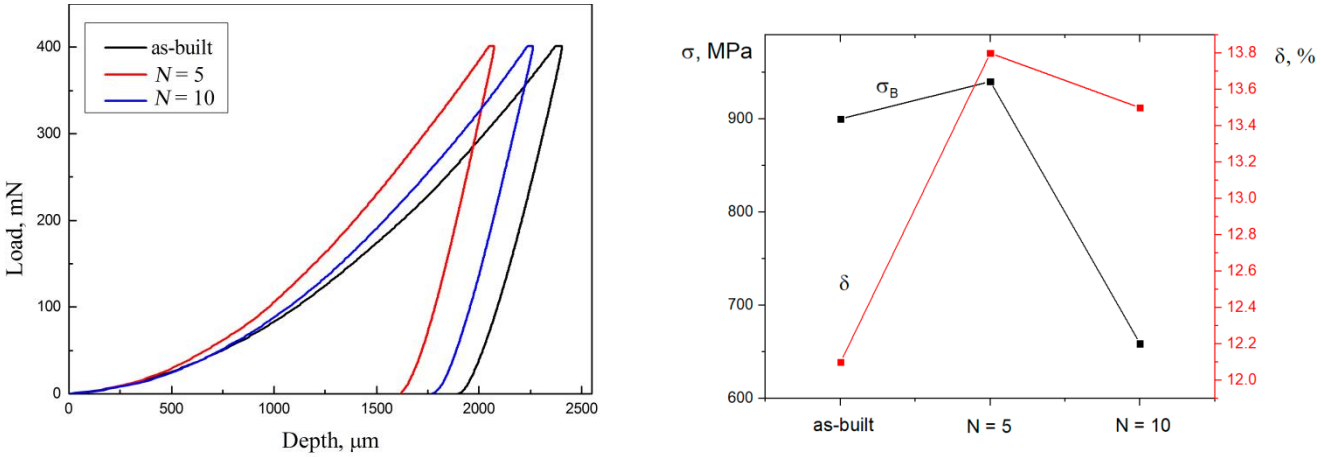

(**a**) (**b**)

Figure 8. (**a**) Load–depth (*F-d*) indentation curves for samples of the EBM Ti-6Al-4V alloy before and after PIB exposure; (**b**) Dependences of ultimate strength (σ_B) and deformation to failure (δ) of the EBM Ti-6Al-4V alloy on the number of irradiation pulses (N).

The results of studying mechanical properties by uniaxial tensile tests of samples of the EBM Ti-6Al-4V alloy are shown in Figure 8b and Table 2. It was found that PIB irradiation has a negligible effect on the plastic characteristics of the EBM Ti-6Al-4V alloy. A decrease in the strength characteristics is observed after irradiation with 10 pulses (Table 2).

Table 2. Mechanical properties of the EBM Ti-6Al-4V alloy in different states.

Samples	$\sigma_{0.2} \pm 20$, MPa	$\sigma_B \pm 20$, MPa	$\delta \pm 0.5$, %
as-built	841	900	12.1
after PIB, N = 5 pulses	823	940	13.8
after PIB, N = 10 pulses	630	659	13.5

Figure 9 represents images of the fracture surface of the samples after tensile tests at room temperature. No significant differences were found between the structures of fracture surfaces for a different series of samples. The fracture pattern of the specimens is viscous and consists of relatively equiaxed "dimples" of various sizes. Fractographic analysis of samples of the EBM Ti-6Al-4V alloy after tension also revealed the presence of single pores with a size of 20 μm.

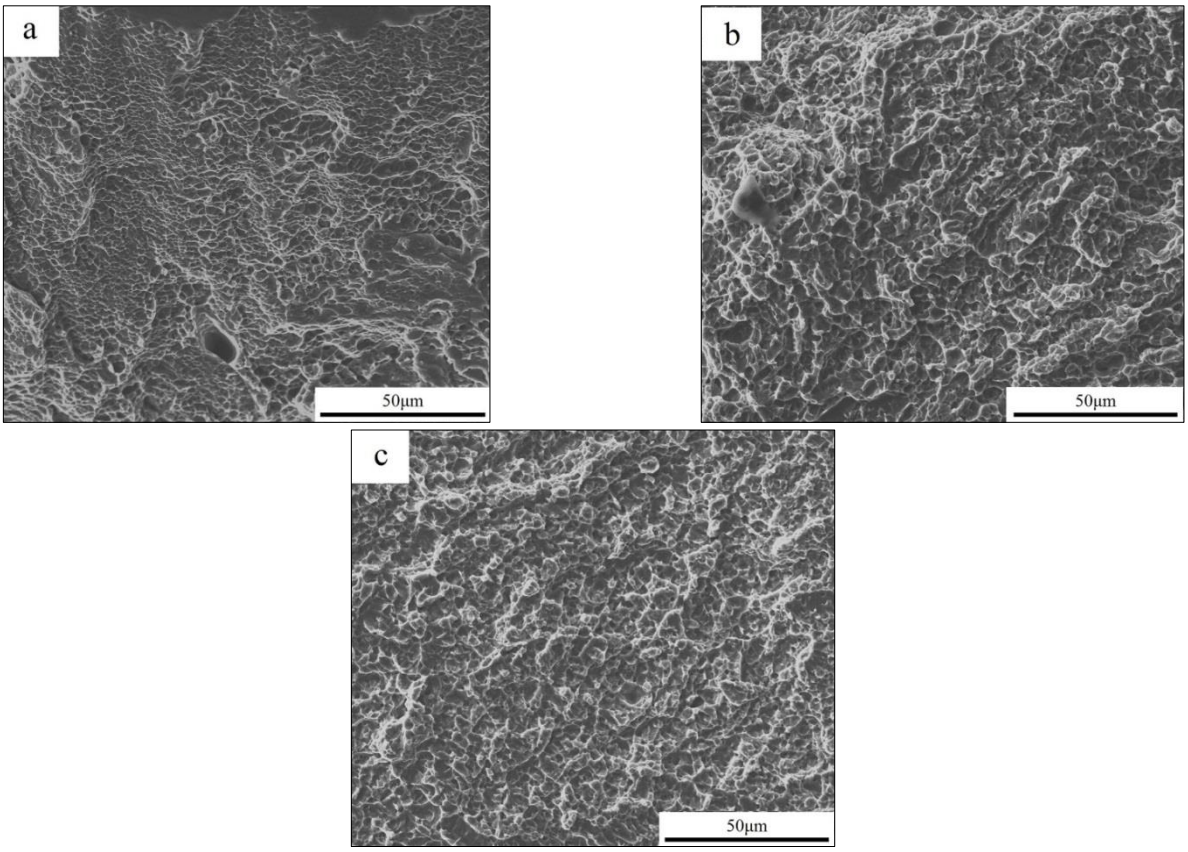

Figure 9. Fracture surfaces of the EBM Ti-6Al-4V alloys: as-built state(**a**); after PIB (N = 5) (**b**); after PIB (N = 10) (**c**).

4. Discussion

The microstructure of the surface layer of the EBM Ti-6Al-4V alloy after exposure to PIB is formed as a result of phase transformations during accelerated cooling from the high-temperature beta region. The high dispersion of the obtained microstructure is caused by the fact that the duration of treatment of the material surface layer in the β regions does not exceed several hundred nanoseconds. In this case, the formation of regions, both supersaturated and depleted in alloying elements, is observed.

During quenching, the depleted part of the β-phase transformed into a low-alloyed α′-martensite, and the enriched β-phase into a more alloyed α″-martensite. This is evidenced by the change in the diffraction patterns of the samples after PIB irradiation, on which the disappearance of the β-phase reflections and the broadening of the α-phase reflections are observed, and onto which the α″-phase reflections can be superimposed (Figure 6). Similar changes in the phase composition of the samples after irradiation with pulsed particle beams were previously observed for the cast Ti-6Al-4V alloy [36]. The formation of the α″-martensite phase in thin surface layers (Figures 4 and 6) is caused by the fact that the formation of the α″-phase requires significantly less atomic displacements compared to the formation of the α′-phase. Small differences in the crystal lattices of martensite and the initial β-phase cause a low activation barrier for the formation of α″-martensite.

The temperature gradient along the depth of the samples leads to the formation of several regions with different microstructures [40]. It was found that twins were the main substructural elements of martensite plates in layer 1 (Figure 4). The presence of twins appears to be the result of the relaxation of internal stresses [41], arising during high-speed quenching from the β-region. The detection of twins in the samples after PIB modification does not contradict the previously obtained data on twinning in hcp alloys [42], since, in these alloys, the tendency for deformation by twinning is determined by the small value of the ratio of the lattice parameters c/a in comparison with bcc and fcc alloys.

The mechanical properties of titanium alloys depend not only on the type of structure (lamellar or globular), but also on the size and shape of the structural components [17,18,43]. With a small intragranular structure, even insignificant changes in the size of the structural components lead to a sharp change in properties. In the case of materials with a microstructure represented by thin long α-plates inside transformed equiaxed β-grains of moderate size, the crack propagates along the boundaries of the primary β-grains and across the colonies of the α-plates, which provides high fracture toughness.

Interesting results are obtained in mechanical tests of materials subjected to high-speed hardening. The redistribution of the concentration of alloying elements, the formation of martensitic phases, and an increase in the dispersion of the structure affect the level of plastic and strength characteristics. The presence of a gradient microstructure along the depth of the material surface layer can provide a better combination of mechanical properties in comparison to materials with a homogeneous structure [36,44]. In the present work, it was found that the exposure of PIB leads to an increase in the values of micro- and nanohardness, which is caused by the formation of a gradient nanostructured state (Figure 4) and the formation of a metastable phase α′. The formation of metastable phases significantly changes the elastic properties of the samples (Table 1). The presence in the surface layers of low-strength α″-martensite, as well as α′-martensite and nanostructured subgrain structure, leads to a change in the mechanical characteristics of the EBM Ti-6Al-4V alloy specimens subjected to modification by PIB (Table 2).

5. Conclusions

It has been demonstrated that modification of the EBM Ti-6Al-4V alloy with a pulsed beam of carbon ions causes significant changes in thin surface layers of the material; depending on the processing mode, it can also improve the mechanical properties of the alloy.

As a result of pulsed ion beam irradiation, a gradient microstructure is formed in the samples of the EBM Ti-6Al-4V alloy. In the surface layer at a depth of about 0.3 μm, the decomposition of the β phase and the formation of twinned martensite α″ are observed. At depths from 0.3 to 4 μm, a mixed microstructure containing alpha-phase plates and acicular martensite is formed. At depths of more than 5 μm, the microstructure practically does not differ from the microstructure of as-built samples.

Modification by a pulsed carbon ion beam with an energy density of 1.92 J/cm^2 and the number of pulses of 5 and 10 leads to an increase in the micro- and nanohardness of the surface layers and a decrease in the wear rate of EBM Ti-6Al-4V alloy during tribological tests.

PIB irradiation (mode 1) of the EBM Ti-6Al-4V alloy surface is found to lead to an increase in the value of ultimate strength, with a simultaneous slight rise in the value of deformation to failure. An increase in the number of processing pulses (mode 2) results in a significant drop in the ultimate strength value (by 27%, compared to as-built samples) of the EBM Ti-6Al-4V alloy, with a practically unchanged high value of deformation to failure.

Author Contributions: Investigation, methodology, writing—original draft preparation, N.P. and E.S.; investigation, A.S.; data curation, M.S. All authors have read and agreed to the published version of the manuscript.

Funding: This research was funded by the Russian Science Foundation, research project №. 17-79-20100.

Institutional Review Board Statement: Not applicable.

Informed Consent Statement: Not applicable.

Data Availability Statement: Data is contained within the article.

Acknowledgments: This work was carried out within the framework of the Competitiveness Enhancement Program of National Research Tomsk Polytechnic University.

Conflicts of Interest: The authors declare no conflict of interest.

References

1. Yusuf, S.M.; Cutler, S.; Gao, N. Review: The Impact of Metal Additive Manufacturing on the Aerospace Industry. *Metals* **2019**, *9*, 1286. [CrossRef]
2. Oliveira, J.; Panton, B.; Zeng, Z.; Andrei, C.; Zhou, Y.; Miranda, R.; Fernandes, F.B. Laser joining of NiTi to Ti6Al4V using a Niobium interlayer. *Acta Mater.* **2016**, *105*, 9–15. [CrossRef]
3. Callegari, B.; Oliveira, J.; Aristizabal, K.; Coelho, R.; Brito, P.; Wu, L.; Schell, N.; Soldera, F.; Mücklich, F.; Pinto, H. In-situ synchrotron radiation study of the aging response of Ti-6Al-4V alloy with different starting microstructures. *Mater. Charact.* **2020**, *165*, 110400. [CrossRef]
4. Murr, L. Metallurgy of additive manufacturing: Examples from electron beam melting. *Addit. Manuf.* **2015**, *5*, 40–53. [CrossRef]
5. Zhang, C.; Chen, F.; Huang, Z.; Jia, M.; Chen, G.; Ye, Y.; Lin, Y.; Liu, W.; Chen, B.; Shen, Q.; et al. Additive manufacturing of functionally graded materials: A review. *Mater. Sci. Eng. A* **2019**, *764*, 138209. [CrossRef]
6. Calleja, A.; Tabernero, I.; Fernández, A.; Celaya, A.; Lamikiz, A.; De Lacalle, L.L.; Mentxaka, A.L.; De Lacalle, L.N.L. Improvement of strategies and parameters for multi-axis laser cladding operations. *Opt. Lasers Eng.* **2014**, *56*, 113–120. [CrossRef]
7. Pushilina, N.; Panin, A.; Syrtanov, M.; Kashkarov, E.; Kudiiarov, V.; Perevalova, O.; Laptev, R.; Lider, A.; Koptyug, A. Hydrogen-Induced Phase Transformation and Microstructure Evolution for Ti-6Al-4V Parts Produced by Electron Beam Melting. *Metals* **2018**, *8*, 301. [CrossRef]
8. Calleja, A.; Tabernero, I.; Ealo, J.A.; Campa, F.J.; Lamikiz, A.; De Lacalle, L.N.L. Feed rate calculation algorithm for the homogeneous material deposition of blisk blades by 5-axis laser cladding. *Int. J. Adv. Manuf. Technol.* **2014**, *74*, 1219–1228. [CrossRef]
9. Sanaei, N.; Fatemi, A. Analysis of the effect of internal defects on fatigue performance of additive manufactured metals. *Mater. Sci. Eng. A* **2020**, *785*, 139385. [CrossRef]
10. Masuo, H.; Tanaka, Y.; Morokoshi, S.; Yagura, H.; Uchida, T.; Yamamoto, Y.; Murakami, Y. Influence of defects, surface roughness and HIP on the fatigue strength of Ti-6Al-4V manufactured by additive manufacturing. *Int. J. Fatigue* **2018**, *117*, 163–179. [CrossRef]
11. Lin, B.; Chen, W.; Yang, Y.; Wu, F.; Li, Z. Anisotropy of microstructure and tensile properties of Ti-48Al-2Cr-2Nb fabricated by electron beam melting. *J. Alloy. Compd.* **2020**, *830*, 154684. [CrossRef]
12. Kok, Y.; Tan, X.; Wang, P.; Nai, M.; Loh, N.; Liu, E.; Tor, S. Anisotropy and heterogeneity of microstructure and mechanical properties in metal additive manufacturing: A critical review. *Mater. Des.* **2018**, *139*, 565–586. [CrossRef]
13. Tan, X.; Kok, Y.; Tan, Y.J.; Descoins, M.; Mangelinck, D.; Tor, S.B.; Leong, K.F.; Chua, C.K. Graded microstructure and mechanical properties of additive manufactured Ti-6Al-4V via electron beam melting. *Acta Mater.* **2015**, *97*, 1–16. [CrossRef]
14. Chern, A.H.; Nandwana, P.; McDaniels, R.; Dehoff, R.R.; Liaw, P.K.; Tryon, R.; Duty, C.E. Build orientation, surface roughness, and scan path influence on the microstructure, mechanical properties, and flexural fatigue behavior of Ti-6Al-4V fabricated by electron beam melting. *Mater. Sci. Eng. A* **2020**, *772*, 138740. [CrossRef]
15. Leon, A.; Levy, G.K.; Ron, T.; Shirizly, A.; Aghion, E. The effect of hot isostatic pressure on the corrosion performance of Ti-6Al-4 V produced by an electron-beam melting additive manufacturing process. *Addit. Manuf.* **2020**, *33*, 101039. [CrossRef]
16. Popov, V.; Katz-Demyanetz, A.; Garkun, A.; Muller, G.; Strokin, E.; Rosenson, H. Effect of Hot Isostatic Pressure treatment on the Electron-Beam Melted Ti-6Al-4V specimens. *Procedia Manuf.* **2018**, *21*, 125–132. [CrossRef]
17. Zhang, X.-Y.; Fang, G.; Leeflang, S.; Böttger, A.J.; Zadpoor, A.A.; Zhou, J. Effect of subtransus heat treatment on the microstructure and mechanical properties of additively manufactured Ti-6Al-4V alloy. *J. Alloy. Compd.* **2018**, *735*, 1562–1575. [CrossRef]
18. Galarraga, H.; Warren, R.J.; Lados, D.A.; Dehoff, R.R.; Kirka, M.M.; Nandwana, P. Effects of heat treatments on microstructure and properties of Ti-6Al-4V ELI alloy fabricated by electron beam melting (EBM). *Mater. Sci. Eng. A* **2017**, *685*, 417–428. [CrossRef]
19. Sabban, R.; Bahl, S.; Chatterjee, K.; Suwas, S. Globularization using heat treatment in additively manufactured Ti-6Al-4V for high strength and toughness. *Acta Mater.* **2019**, *162*, 239–254. [CrossRef]
20. Panin, A.; Kazachenok, M.; Perevalova, O.; Martynov, S.; Panina, A.; Sklyarova, E. Continuous Electron Beam Post-Treatment of EBF^3-Fabricated Ti-6Al-4V Parts. *Metals* **2019**, *9*, 699. [CrossRef]
21. Farayibi, P.; Abioye, T.; Murray, J.; Kinnell, P.; Clare, A. Surface improvement of laser clad Ti-6Al-4V using plain waterjet and pulsed electron beam irradiation. *J. Mater. Process. Technol.* **2015**, *218*, 1–11. [CrossRef]
22. Tian, Y.; Gora, W.S.; Cabo, A.P.; Parimi, L.L.; Hand, D.P.; Tammas-Williams, S.; Prangnell, P.B. Material interactions in laser polishing powder bed additive manufactured Ti6Al4V components. *Addit. Manuf.* **2018**, *20*, 11–22. [CrossRef]
23. Hao, S.; Qin, Y.; Mei, X.; Gao, B.; Zuo, J.; Guan, Q.; Dong, C.; Zhang, Q. Fundamentals and applications of material modification by intense pulsed beams. *Surf. Coat. Technol.* **2007**, *201*, 8588–8595. [CrossRef]
24. Ryabchikov, A. Progress in low energy high intensity ion implantation method development. *Surf. Coat. Technol.* **2020**, *388*, 125561. [CrossRef]
25. Li, P.; Peng, T. Surface morphology of magnesium alloy irradiated by high-intensity pulsed ion beam. *Appl. Surf. Sci.* **2012**, *258*, 9961–9968. [CrossRef]
26. Chernov, I.P.; Beloglazova, P.A.; Berezneeva, E.V.; Kireeva, I.V.; Pushilina, N.S.; Remnev, G.E.; Stepanova, E.N. Properties of the VT1-0 titanium surface modified by a pulsed ion beam. *Tech. Phys.* **2015**, *60*, 1039–1043. [CrossRef]

27. Struts, V.; Zakoutaev, A.; Matvienko, V.; Petrov, A.; Shlapakovski, A. Formation of protective coatings on metals by intense pulsed ion beam. *Surf. Coat. Technol.* **2002**, *158*, 494–497. [CrossRef]
28. Shulov, V.; Nochovnaya, N. Fatigue strength of metals and alloys modified by ion beams. *Surf. Coat. Technol.* **2002**, *158*, 33–41. [CrossRef]
29. Pogrebnjak, A.; Remnev, G.; Kurakin, I.; Ligachev, A. Structural, physical and chemical changes induced in metals and alloys exposed to high power ion beams. *Nucl. Instrum. Methods Phys. Res. Sect. B Beam Interact. Mater. Atoms* **1989**, *36*, 286–305. [CrossRef]
30. Lavrentiev, V.; Hammerl, C.; Rauschenbach, B.; Kukharenko, O. Formation of hardened surface layers in titanium under irradiation with intense ion beams. *Scr. Mater.* **2001**, *44*, 625–630. [CrossRef]
31. Renk, T.; Provencio, P.; Prasad, S.; Shlapakovski, A.; Petrov, A.; Yatsui, K.; Jiang, W.; Suematsu, H. Materials modification using intense ion beams. *Proc. IEEE* **2004**, *92*, 1057–1081. [CrossRef]
32. Zou, H.; Zhang, L.; Guan, T.; Zhang, X.; Remnev, G.E.; Pavlov, S.K.; Wang, Y.; Mei, X. Effect on mechanics properties and microstructure of molybdenum by high intensity pulsed ion beam irradiation. *Surf. Coat. Technol.* **2020**, *384*, 125333. [CrossRef]
33. Remnev, G.; Uglov, V.; Shymanski, V.; Pavlov, S.; Kuleshov, A. Formation of nanoscale carbon structures in the surface layer of metals under the impact of high intensity ion beam. *Appl. Surf. Sci.* **2014**, *310*, 204–209. [CrossRef]
34. Lei, M.; Dong, Z.; Zhang, Z.; Hu, Y.; Zhu, X. Wear and corrosion resistance of Ti6Al4V alloy irradiated by high-intensity pulsed ion beam. *Surf. Coat. Technol.* **2007**, *201*, 5613–5616. [CrossRef]
35. Wang, X.; Han, X.; Lei, M.; Zhang, J. Effect of high-intensity pulsed ion beams irradiation on corrosion resistance of 316L stainless steel. *Mater. Sci. Eng. A* **2007**, *457*, 84–89. [CrossRef]
36. Grabovetskaya, G.P.; Stepanova, E.N.; Mishin, I.P.; Zabudchenko, O.V. The Effect of Irradiation of a Titanium Alloy of the Ti-6Al-4V-H System with Pulsed Electron Beams on Its Creep. *Russ. Phys. J.* **2020**, *63*, 932–939. [CrossRef]
37. Pushilina, N.S.; Klimenov, V.A.; Cherepanov, R.O.; Kashkarov, E.B.; Fedorov, V.V.; Syrtanov, M.S.; Lider, A.M.; Laptev, R.S. Beam Current Effect on Microstructure and Properties of Electron-Beam-Melted Ti-6Al-4V Alloy. *J. Mater. Eng. Perform.* **2019**, *28*, 6165–6173. [CrossRef]
38. Stepanov, A.V.; Shamanin, V.I.; Remnev, G.E. The study of operation modes of the self-magnetically insulated ion diode. *Rev. Sci. Instrum.* **2019**, *90*, 033302. [CrossRef] [PubMed]
39. Stepanova, E.; Grabovetskaya, G.; Syrtanov, M.; Mishin, I. Effect of Hydrogen on the Deformation Behavior and Localization of Plastic Deformation of the Ultrafine-Grained Zr—1Nb Alloy. *Metals* **2020**, *10*, 592. [CrossRef]
40. Boiko, V.I.; Valyaev, A.N.; Pogrebnyak, A.D. Metal modification by high-power pulsed particle beams. *Phys. Uspekhi* **1999**, *42*, 1243–1271. [CrossRef]
41. Li, C.; Li, G.; Yang, Y.; Varlioglu, M.; Yang, K. α" Martensitic Twinning in Alpha + Beta Ti-3.5Al-4.5Mo Titanium Alloy. *J. Metall.* **2011**, *2011*, 924032. [CrossRef]
42. Kelly, A.; Growes, G.W. *Crystallography and Crystal Defects*; Longman: London, UK, 1970.
43. Sieniawski, J.; Ziaja, W.; Kubiak, K.; Motyka, K.K.A.M. *Microstructure and Mechanical Properties of High Strength Two-Phase Titanium Alloys*; BoD—Books on Demand: Norderstedt, Germany, 2013; pp. 69–80. [CrossRef]
44. Ma, X.; Li, F.; Sun, Z.; Hou, J.; Fang, X.; Zhu, Y.; Koch, C.C. Achieving Gradient Martensite Structure and Enhanced Mechanical Properties in a Metastable β Titanium Alloy. *Metall. Mater. Trans. A* **2019**, *50*, 2126–2138. [CrossRef]